Transport in Porous Media **35:** 67–88, 1999.

A Multiscale Network Model for Simulating Moisture Transfer Properties of Porous Media

JAN CARMELIET[1], FILIP DESCAMPS[2] and GEERT HOUVENAGHEL[1]
[1]*Department of Civil Engineering, Catholic University of Leuven, Celestijnenlaan 131, B-3001 Heverlee, Belgium*
[2]*Daidalos Building Physics Engineering, Rodenbachstraat 71, B-3010 Leuven, Belgium*

(Received: 9 July 1997; in final form: 13 July 1998)

Abstract. A multiscale network model is presented to model unsaturated moisture transfer in hygroscopic capillary-porous materials showing a broad pore-size distribution. Both capillary effects and water sorption phenomena, water vapour and liquid water transfer are considered. The multiscale approach is based on the concept of examining the porous space at different levels of magnification. The conservation of the water vapour permeability of dry material is used as scaling criterion to link the different pore scales. A macroscopic permeability is deduced from the permeabilities calculated at the different levels of magnification. Each level of magnification is modelled using an isotropic nonplanar 2D cross-squared network. The multiscale network simulates the enhancement of water vapour permeability due to capillary condensation, the hysteresis phenomenon between wetting and drying, and the steep increase of moisture permeability at the critical moisture saturation level. The calculated network permeabilities are compared with experimental data for calcium silicate and ceramic brick and a good agreement is observed.

Key words: multiscale network, moisture permeability, water vapour diffusion, liquid water transfer.

1. Introduction

The main mechanisms of moisture transfer in hygroscopic capillary-porous materials consist of both water sorption phenomena and capillary effects. Moisture transfer includes the simultaneous movement of water vapour and liquid water in porous material. Examples of such materials are ceramic bricks, cementitious materials and natural stones, all of which contain a broad range of pore radii ranging from 1×10^{-9} to 1×10^{-2} m. At low relative humidities, liquid water only forms a very thin film of adsorbed water on the pore walls, with a thickness of some molecules. This film adheres strongly to the pore wall and is practically immobile. Moisture transfer processes in this low moisture saturation range are dominated by molecular vapour diffusion, Knudsen diffusion and bulk flow of the gas phase. As moisture saturation increases, wetting fluid fills the smaller pores, creating dispersed water-filled regions through capillary condensation. Liquid water transfer in water-filled regions is far more efficient, resulting in an apparent enhancement of the experimentally observed water vapour flow (Philip and de Vries, 1957). As moisture saturation further increases,

water-filled regions expand and coalesce until, at some critical moisture saturation level, a continuous liquid water phase is formed. At this critical point, a steep increase of the moisture permeability is experimentally observed. In hygroscopic capillary-porous material with broad pore-size distribution, strong entrapment and hysteresis phenomena between adsorption and desorption naturally appear due to the complex connectivity between different pore scales. As a consequence, the moisture transfer properties of hygroscopic capillary-porous materials are highly dependent on the moisture saturation level and hysteresis phenomena.

In this paper a network model is developed to model the relevant moisture transfer phenomena in hygroscopic capillary-porous materials showing a broad pore-size distribution. Network models were initially introduced by Fatt (1956) and combined with percolation concepts (see for example Diaz *et al.*, 1987; Sahimi, 1993). To quote only a few representative contributions in this field, we mention lattices composed of sites and bonds (used for example by Koplik, 1982; Koplik and Lasseter, 1985; Constantinidis and Payatakes, 1989; Blunt *et al.*, 1992; Soll and Celia, 1993), lattices composed of volumeless intersections (Fatt, 1956; Wise, 1992; Sahimi, 1993), bond-correlated site percolation in random networks (Diaz *et al.*, 1987; Ioannidis and Chatzis, 1993), invasion percolation (Wilkinson and Willemsen, 1988; Chandler *et al.*, 1982; Lenormand *et al.*, 1988), invasion percolation in combination with vapour transfer (Prat, 1995).

To describe porous building materials with broad pore-size distributions, multi-scale pore models have been introduced (Neimark, 1989). In the multiscale approach the pore space is described as a superposition of several pore subsystems situated at different pore-size ranges. A crucial point is the modelling of the interconnection between the different scales. Xu *et al.* (1997) used hierarchic lattices, in which networks of lower pore-size range are connected to larger scales using rescaling and normalisation techniques (Wilson, 1971).

In this paper, we propose a multiscale approach based on the concept of examining the porous space at different levels of magnification. A scaling technique and selection criterion is developed to link the macroscopic permeability to the permeabilities calculated at the different levels of magnification. The constitutive networks at the sublevels are isotropic nonplanar 2D cross-squared networks and no correlation is assumed. Only static configurations of networks filled by water vapour and liquid water are considered. Clearly, the emphasis here is on the multiscale concept. However, the concept can be applied to more sophisticated pore network models. The influence of the nature of the network on the multiscale model is still to be studied.

First, the multiscale network model is presented and the influence of the network parameters on the predicted moisture permeability is studied. Then, the network model is validated through comparison with experimental data.

2. Multiscale Approach

2.1. REPRESENTING THE PORE SPACE

Typical pore volume distributions of hygroscopic capillary-porous materials, such as ceramic brick and calcium silicate, are shown in Figure 1. The broad pore-size distribution is composed of a pore system of coarse pores (equivalent pore radius $r \geqslant 1\,\mu$m) and a secondary pore system of fine and mid-size pores ($10^{-3}\,\mu\text{m} \leqslant r \leqslant 1\,\mu$m). The SEM micrograph in Figure 2 shows the pore structure for ceramic brick (resolution: $r \geqslant 0.5\,\mu$m). At this level of magnification, the pore space consists of interconnected coarse pores intersecting blocks of finer porous material. At low degrees of moisture saturation, only the blocks of finer porous material are filled with water. In this case, moisture transfer consists of water vapour transfer through the coarse pore space and liquid water transfer in the fine pore space of the blocks. Since liquid water transfer is far more efficient, this results in an apparent enhancement of the macroscopic water vapour flow. The coarse pores intersecting the blocks of fine porous material interrupt the continuous liquid water phase in the finer pore space of the blocks, resulting in a decrease of liquid water permeability of the blocks. With increasing degree of saturation, the coarse pores themselves become gradually filled with water and form a continuous liquid water phase. At this point, nearly all moisture transfer will take place in the coarse pore system, resulting in a steep increase of the moisture permeability.

It is important to note that the observed porous structure as shown in Figure 2 is only representative for the SEM scale of observation ($r \geqslant 0.5\,\mu$m). Information on the pore space at lower levels is hard to determine experimentally. Therefore, in a first approximation we will assume that the porous structure at higher magnifications is of a similar nature as the porous structure at the SEM scale. The multiscale model will attempt to reproduce the above mentioned relevant moisture transfer phenomena

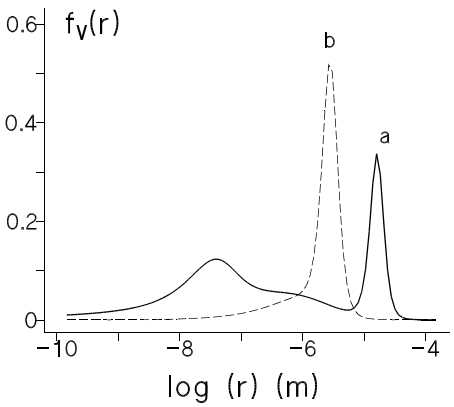

Figure 1. Pore volume distribution $f_V(r)$ for two hygroscopic capillary-porous materials: (a) calcium silicate, and (b) ceramic brick.

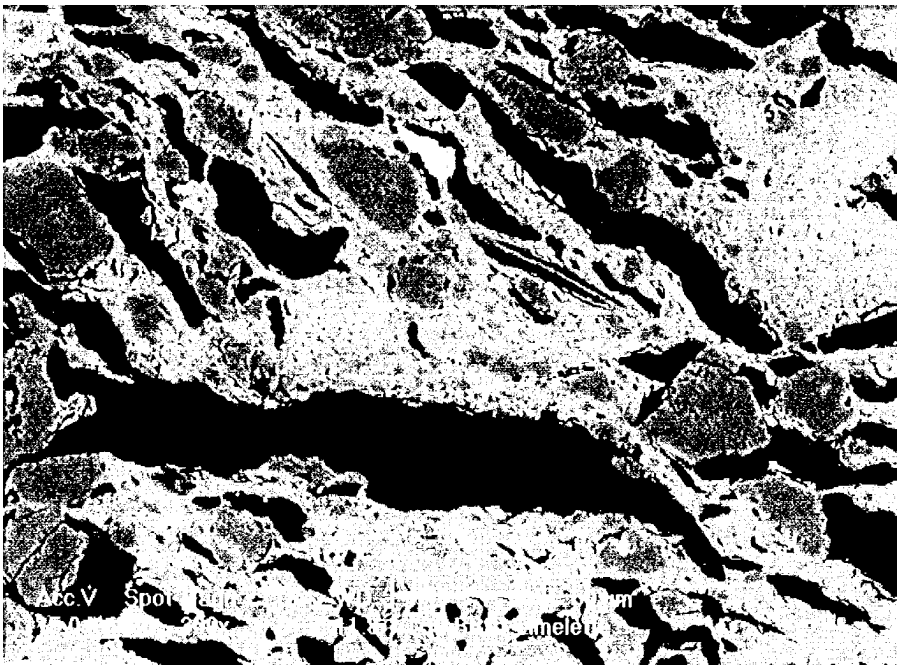

Figure 2. SEM micrograph of ceramic brick, showing the pores in black. The baseline is 360 μm.

at the different pore scales. It is not constructed as an accurate representation of the porous structure itself.

Figure 3 shows two different concepts of multiscale approaches for a porous medium with broad pore-size distribution. In the first concept (Xu *et al.*, 1997) the medium is described as a superposition of network models representing the various pore classes of the material (Figure 3(b)). The lower pore classes are rescaled and incorporated into a renormalised network. The number of pore classes is set by a fixed scaling factor. The volumetric concentrations and pore-size distributions at the different scales are indirectly identified from measurements.

The multiscale approach, proposed in this paper, is schematically illustrated in Figure 3(c). Different scales of observation are considered by looking at the porous material at different levels of magnifications. By gradually reducing the level of observation (increasing magnification), information of coarse pore systems dissipates and detailed information of finer pore systems becomes discernible. The pore space at each level of magnification is characterised by a volumetric porosity ϕ_i and a pore-size distribution f_i. A network model is used to determine the permeability at each level of magnification. Using a scaling criterion the permeabilities are incorporated into a macroscopic moisture permeability curve.

In contrast with the first multiscale approach (Xu *et al.*, 1997), the problem of defining different pore classes is circumvented. The problem now concentrates

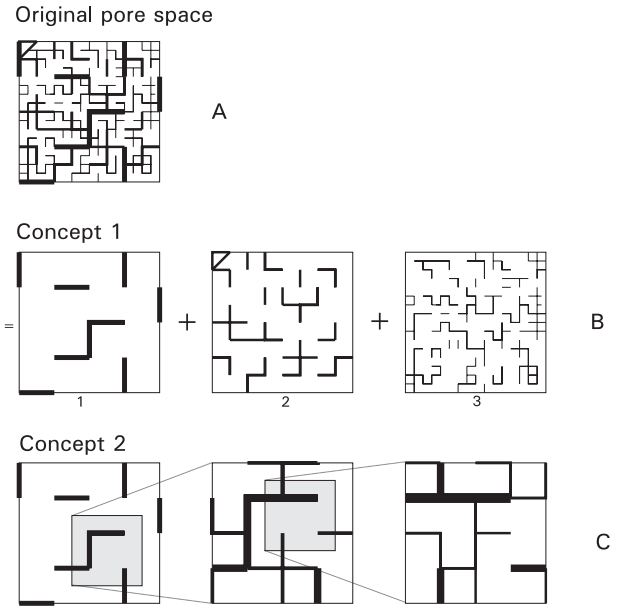

Figure 3. Schematic representation of two concepts of multiscale network: (a) original pore space, (b) concept 1: the pore space is described as a superposition of three pore classes, and (c) concept 2: different scales of observation by looking at the porous material at different levels of magnification.

on identifying the porosities and pore-size distributions for the different levels of magnification.

The equivalent pore radius distribution f_R is determined from the measured water retention curve $S = S(p_c(r))$:

$$f_R(r) = \frac{1}{\rho_1} \frac{\partial w}{\partial \log_{10}(r)} \frac{1}{\pi r^2 L} = -\phi_0 \frac{\partial S}{\partial \log_{10}(p_c)} \frac{1}{\pi r^2 L}, \tag{1}$$

where r is the equivalent pore radius, w the total volumetric moisture content, S the level of saturation, p_c the capillary pressure (definitions see appendix), ϕ_0 the total open porosity, ρ_l the volumetric density of water and L the cylindrical pore length. In Equation (1), we used the Laplace equation

$$r = \frac{2\sigma \cos\beta}{p_c}, \tag{2}$$

where σ is the water-moist air surface tension, and β the contact angle of the solid-water-moist air mixture.

Next, a pore shape has to be assumed to calculate the pore radius distribution $f_R(r)$ from the measured pore volume distribution. We introduce a pore shape ratio α, which defines the pore length L as a function of the pore tube radius r:

$$L(r) = L_M \left(\frac{r}{r_M} \right)^{\alpha}, \tag{3}$$

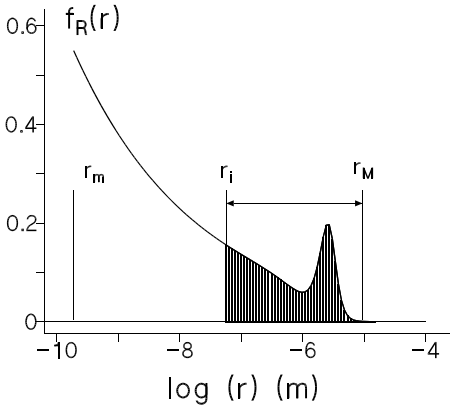

Figure 4. Pore radius distribution $f_R(r)$ of ceramic brick with pore shape ratio $\alpha = -1$. The dashed area represents the pore range observed at the ith level of magnification $[r_i, r_M]$, with r_i the cut-off radius.

where L_M is a reference tube length for the pore with maximal radius r_M of the pore system. As an example, the pore radius distribution with $\alpha = -1$ for ceramic brick is illustrated in Figure 4.

At a certain level of magnification, we only consider the pore space in a pore radius range $[r_i, r_M]$. The cut-off radius r_i is defined as the lower limit of the pore-size range $[r_i, r_M]$ observed at the ith level of magnification. The porosity ϕ_i and the number of pores n_i are

$$\phi_i = \phi_0(1 - S(r_i)), \qquad n_i = \int_{r_i}^{r_M} f_R(r)\,\mathrm{d}\,\log(r). \tag{4}$$

The normalised pore radius distribution f_i^{n} used in the network modelling is

$$f_i^{\mathrm{n}}(r) = \frac{f_R(r)}{n_i}, \quad r \in [r_i, r_M]. \tag{5}$$

We emphasize that the normalised pore radius distribution is independent of the length L_M. Figure 5 gives the normalised pore radius distribution for different levels of magnification. As an example, Figure 6 shows 2D square network representations for two levels of magnification. At low level of magnification, the network simulation only includes information of the coarse pore space. Therefore, the calculated permeability at complete saturation will only depend on the coarse pore space, which is mainly in agreement with experimental findings. At high level of magnification, the network model includes information on the fine pores as well as on some coarse pore intersecting the fine porous space. The presence of coarse pores in the finer porous blocks is in agreement with SEM observations (Figure 2). The intersecting coarse pores will block the liquid water transfer in the fine pores space resulting in a lower permeability. Moreover, the coarse pores will not be readily accessible to the outside atmosphere during desorption, which results in hysteresis between adsorption

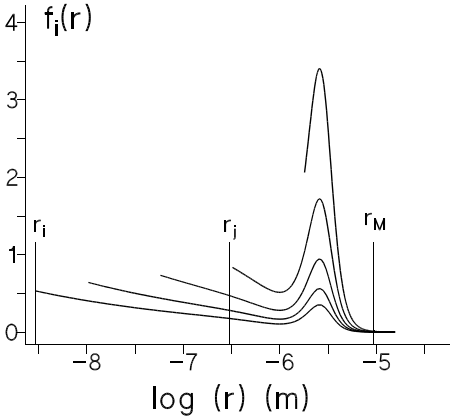

Figure 5. Normalised pore radius distributions for different levels of magnifications.

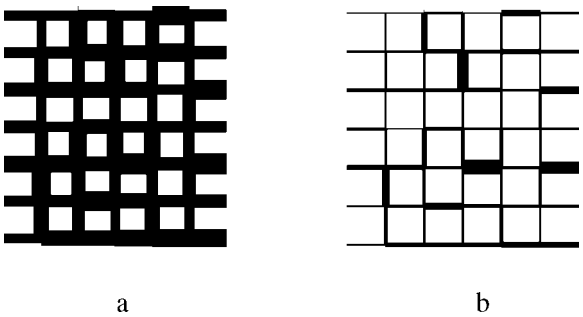

Figure 6. Schematic 2D network representations at two levels of magnification. At high levels of magnification (a) the network model only includes coarse pores. At low level of magnification (b) only a few coarse pores show up in the fine porous network.

and desorption. It is obvious that at low (respectively high) levels of magnification the simulation includes insufficient pore space information to accurately simulate the permeability at low (respectively high) saturations. This means that an optimal level of magnification $[r_i, r_M]$ needs to be found to predict the permeability at a certain level of saturation or capillary pressure p_c. This issue will be addressed in Section 2.3.

2.2. NETWORK MODEL

Each level of magnification $[r_i, r_M]$ with its normalised radius distribution f_i^{n} is simulated using a network model. For simplification, uncorrelated and isotropic networks have been chosen. Therefore, the network model in its present form cannot be applied to porous materials showing a strong spatial organisation of the pore space. However, when information on the correlation structure of the pore space at different scales of magnification is available, the concept of multiscale approach as proposed in the previous paragraph can still be applied.

The network model used is a 2D nonplanar lattice with volumeless intersections. In nonplanar models, the liquid water traverses the model during imbibition without disconnecting the mixture of water vapour and dry air. Nonplanar networks have shown to capture the most important features of 3D pore structures (Constantinides and Payatakes, 1989). Examples of nonplanar 2D networks are triangular and crossed square lattices. In order to combine the computational economy of a 2D lattice and the crucial topological characteristics of 3D lattices, a cross-squared 2D lattice has been chosen. Using a typical Monte Carlo simulation the radius of a tube element in the lattice is selected at random from the normalised pore radius distribution $f_i^{\mathrm{n}}(r)$. It is important to note that the concept of the present multiscale approach is not limited to the network model used in this paper, but can be applied to different network models as well.

In the static network approach, the basic rule for water-filling of a tube in the network is the Laplace formula (Equation (2)) (Dullien, 1979). In the wetting regime a network tube is assumed to become water-filled if its radius r is smaller than the radius $r(p_c)$ as given by the Laplace equation. The tubes which are not filled by water are assumed to be filled with a mixture of water vapour and dry air. The very thin wetting film adsorbed on the tube surface is not included in the model, since the surface flow in this adsorbed water film layer is of less importance (Kamp, 1988). In the drying regime, we consider the following accessibility rule: only those pores which show a traceable air path to the atmosphere may desorb.

The liquid water and water vapour flow in a cylindrical tube are described by appropriate constitutive relations. The incompressible laminar liquid water flow in a water-filled tube with radius r and length L is described by the Hagen–Poiseuille equation

$$\dot{m}_{\mathrm{l}} = -k_{\mathrm{l}} \frac{\Delta p_{\mathrm{l}}}{L} = -\left(\frac{\rho_{\mathrm{l}} r^2}{8\eta_{\mathrm{l}}} \right) \frac{\Delta p_{\mathrm{l}}}{L}, \tag{6}$$

where p_{l} is the liquid water pressure, k_{l} the liquid water tube permeability and η_{l} the dynamic viscosity. The water vapour flow through a tube with length L may be described by a Fickian law

$$\dot{m}_{\mathrm{v}} = -k_{\mathrm{v}} \frac{\Delta p_{\mathrm{v}}}{L} = -\left(\frac{D_{\mathrm{va}}}{1 + N_{\mathrm{k}}} \frac{1}{R_{\mathrm{v}} T} \right) \frac{\Delta p_{\mathrm{v}}}{L}, \tag{7}$$

where p_{v} is the water vapour pressure, k_{v} the water vapour tube permeability, R_{v} the universal gas constant for water vapour and T the absolute temperature. The binary molecular diffusion coefficient D_{va} accounts for the interaction between the gas molecules (Schirmer, 1938)

$$D_{\mathrm{va}} = 2.31 \times 10^{-5} \frac{p_{\mathrm{atm}}}{p_{\mathrm{atm}} + p_{\mathrm{v}}} \left(\frac{T}{273.16} \right)^{1.81}, \tag{8}$$

where p_{atm} is the atmospheric pressure. The Knudsen number N_{k} accounts for the interaction of the gas molecules with the pore walls of very fine pores and equals

$N_k = l_m/2r$, with l_m the mean free path length of the gas molecules (5×10^{-8} m). We assume that water vapour diffusion does not occur in nanometre size pores, which are of the size of a water molecule and are virtually inaccessible to water vapour molecules. This radius is taken as the minimal radius of the pore system, or, $r_m = 1 \times 10^{-9}$ m. Assuming the Kelvin–Laplace equation is valid at the vapour-liquid interface (see Appendix), the vapour permeability k_v can be converted into an equivalent liquid permeability k_v^l related to a gradient in capillary pressure

$$k_v^l = k_v p_{vs} \frac{\partial h}{\partial p_c}, \tag{9}$$

where h is the relative humidity and p_{vs} is the water vapour saturation pressure. Note that for isobaric and isothermal conditions the permeability k_v^l is independent of the tube radius r and thus only dependent on the capillary pressure.

Given the fluid distribution in the network corresponding to a known capillary pressure p_c, the permeability can be calculated by imposing a unit pressure gradient at two opposite sides of the network, while at the other sides no-flow conditions are imposed. To obtain multiple results for statistical testing and ensemble averaging, the entire process is repeated for different lattice simulations. The average moisture permeability depends linearly on the length parameter L_M and is therefore called relative permeability K_r. By incrementally increasing (or decreasing) the capillary pressure the average permeability versus capillary pressure relation $K_r(p_c)$ for one level of magnification can be determined.

2.3. RESCALING

By gradually increasing the level of magnification, a set of relative permeabilities K_r^i as a function of capillary pressure p_c is determined. To obtain one macroscopic permeability curve we have to overcome two additional difficulties. First, the relative permeability for each level of observation has to be scaled to an absolute permeability K^i. Therefore, a scaling coefficient a_i is introduced $K^i = a_i K_r^i$. A procedure to determine this scaling coefficient is presented later in this section. Second, from the permeability curves at different levels of magnification a global permeability curve has to be deduced. The latter problem is related to the evaluation of the optimal level of magnification $[r_i, r_M]$ for the calculation of the permeability at a given capillary pressure p_c. As an example, Figure 7(a) shows the calculated average relative moisture permeability as a function of pore radius $r(p_c)$ for two pore systems, with cut-off radii r_i and r_j. We notice that the pore system $[r_i, r_M]$ only contributes to the moisture permeability in a limited pore range $[r_i, r_1]$. At values of $r(p_c) < r_i$, all pores are filled with water vapour and the water vapour permeability at zero saturation $K_{S=0}$ is recovered. At values of $r(p_c) > r_1$ only a relatively negligible number of coarse pores become water-filled and no significant increase of the moisture permeability is observed. If we perform the same calculation at magnification level j the permeability is underestimated in a certain range near

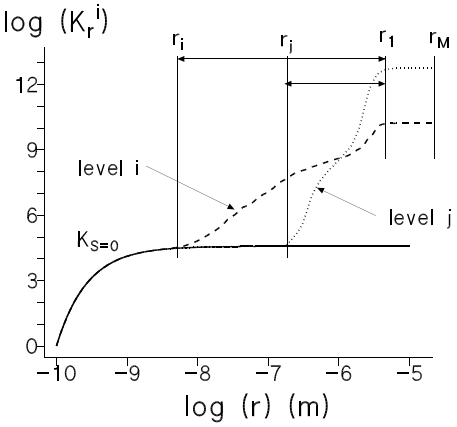

Figure 7a. Simulated moisture permeability for the pore system at level of magnification i and j. The ranges $[r_i, r_1]$ and $[r_j, r_1]$ represent the active pore radius ranges where the pore system is contributing to the moisture permeability. Also the water vapour permeability $K_{S=0}$ is indicated.

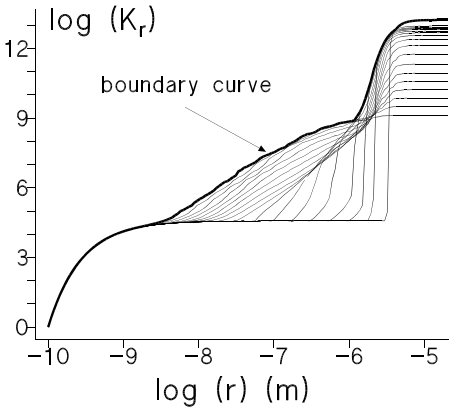

Figure 7b. Global relative permeability curve determined as the upper boundary curve to the scaled permeability curves at different levels of magnification.

the cut-off radius r_j compared to the calculation at level i. Reason for this is that the number of pores filled with water by capillary condensation is underestimated near the cut-off radius r_j. Similarly, magnification level i underestimates the permeability at the radius r_1 because it underestimates the coarse pore distribution. Since the permeability cannot be overestimated, the macroscopic permeability curve can be determined as the upper boundary curve of the permeability curves at different levels of magnification, or

$$K(p_c) = \max[a_i K_{\mathrm{r}}^i(p_c)], \quad i = 1, \ldots, M, \tag{10}$$

where M is the number of levels of magnification. To evaluate the scaling coefficient a_i, a scaling criterion has to be defined. According to Equation (9), the calculated

water vapour permeability at zero saturation $K_{S=0}$ is independent of the pore radius distribution, but only dependent on the capillary pressure and the porosity ϕ_i. The conservation of the water vapour permeability $K_{S=0}$ for the different levels of observation thus implies that

$$K_{S=0} = a_0 K_r^0(p_m) = a_i K_{\mathrm{r}}^i(p_m) \tag{11}$$

or

$$a_i = a_0 \frac{K_{\mathrm{r}}^0(p_m)}{K_{\mathrm{r}}^i(p_m)}, \tag{12}$$

where p_m is the capillary pressure at the minimal pore radius r_m, or, $p_m = p_c(r_m)$. The index 0 refers to the highest level of magnification. This scaling procedure corresponds to a scaling of the network porosity ϕ_i to the open porosity ϕ_0 of the porous material. As an example, Figure 7(b) shows the global relative permeability curve determined as the upper boundary curve to the scaled permeability curves at different levels of magnification. The scaling coefficient a_0 can be obtained by matching the maximal value of the moisture permeability to the measured moisture permeability at complete saturation $K_{S=1} = a_0 K_{\mathrm{r}}(p_M)$, with $p_M = p_c(r_M)$. The absolute saturated moisture permeability $K_{S=1}$ may be identified by the measurement of the air permeability of the dry material $K_{\mathrm{a},S=0}$:

$$K_{S=1} = \frac{\rho_{\mathrm{l}} \eta_{\mathrm{a}}}{\rho_{\mathrm{a}} \eta_{\mathrm{l}}} K_{\mathrm{a},S=0}. \tag{13}$$

3. Numerical Results

In this section the influence of the network parameters (the connectivity z, the network size s, the pore shape ratio α and the number of simulations n) on the predicted moisture permeability is analysed. For the model behaviour analysis the reference data of Table 1 (ceramic brick) are used.

We first analyse the minimum network size s and the number of simulations n required to obtain an accurate estimate of the mean saturated moisture permeability $K_{s=1}$. The network size s for square networks is defined as the number of tubes in each dimension. Using the student's distribution, a confidence interval $[K_{s=1}-d,\ K_{s=1}+d]$ in which the true mean can be found with a given probability p, can be calculated. The confidence interval limit d is given by

$$d = t(p, n) \frac{\sigma}{\sqrt{n}}, \tag{14}$$

where n is the number of simulations, σ the sample standard deviation and t the student's distribution value for a given confidence level p. Figure 8 shows the influence of the network size s on the 95% confidence interval d for different numbers of simulations n. In general, the required number of simulations n for a certain value

Table I. Distribution parameters, reference multiscale network model parameters and basic moisture properties for calcium silicate brick and ceramic brick

	Calcium silicate	Ceramic brick
Distribution parameters		
Number of distributions	3	2
Parameter c_1	3.55×10^{-7}	9.77×10^{-6}
Parameter c_2	1.19×10^{-5}	2.00×10^{-5}
Parameter c_3	1.15×10^{-4}	
Exponent n_1	2.026	1.78
Exponent n_2	1.238	5.5
Exponent n_3	6.299	
Weight factor l_1	0.27	0.25
Weight factor l_2	0.46	0.71
Weight factor l_3	0.27	
Vacuum saturation moisture content w_{sat} (kg/m^3)	359	242
Multiscale network model parameters		
Network size s	30	30
Simulation number n	40	40
Pore shape ratio α	-1	-1
Connectivity z	8	8
Maximal pore radius r_m (m)	48.0×10^{-6}	15.8×10^{-6}
Minimal pore radius r_M (m)	1.0×10^{-9}	1.0×10^{-9}
Basic moisture properties		
Bulk density ρ (kg/m^3)	1689	2005
Open porosity φ_0	0.359	0.24
Saturated water permeability $K_{s=1}$ (s)	7.9×10^{-8}	1.3×10^{-7}
Capillary moisture content w_{cap} (kg/m^3)	260	157

of the confidence interval decreases with increasing network size s. A network size of $s = 30$ and a number of simulations $n = 40$ was found to be the optimal choice with regard to computational effort and accuracy. The obtained accuracy is a confidence interval d of 2% of the mean saturated moisture permeability $K_{S=1}$.

Different values of the pore shape ratio α have been used in literature: $\alpha = 1$ (Wise, 1992), $\alpha = 0$ (Constantinides and Payatakes, 1989; Lenormand *et al.*, 1988; Quenard, 1989) and $\alpha = -1$ (Descamps, 1997; Fatt, 1956). In order to study the influence of the pore shape factor, the moisture permeability $K(p_c)$ was calculated

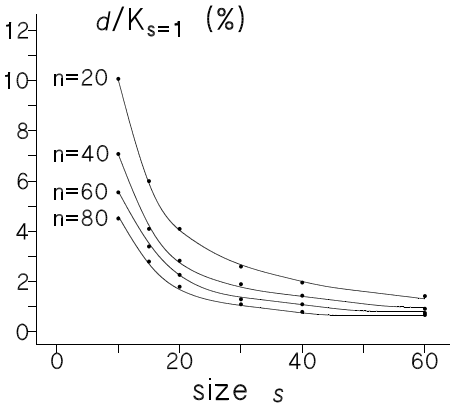

Figure 8. Student's t-confidence intervals with a confidence level $p = 0.95$ for different network sizes s and number of simulations n. As the network size s increases, the required number of simulations n decreases.

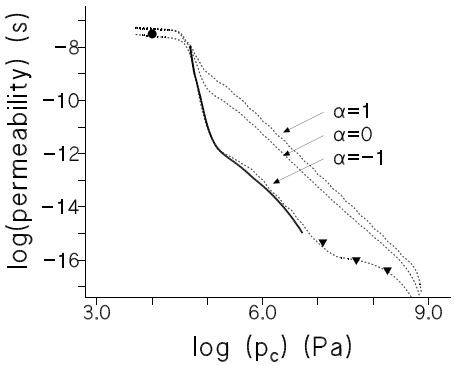

Figure 9. Influence of the pore shape ratio α on the permeability. A pore shape ratio $\alpha = -1$ reasonably agrees with the experimental results for ceramic brick: •, saturated moisture permeability calculated from the measured dry air permeability; –, NMR; ▼, wet cup/dry cup vapour permeability.

for three values of α (Figure 9). The moisture permeability $K(p_c)$ is found to be rather sensitive to the pore shape factor α. For high values of α, a mainly exponential relationship is found between the moisture permeability and the capillary pressure. For lower values of α, the permeability curves show a steep increase at a capillary pressure threshold, also referred to as the critical moisture saturation.

A characteristic property of a network model is its connectivity z, which is defined as the number of tubes connected to a node. Measurements of the connectivity were done on Berea sandstone by Lin and Cohen (1982) showing that the connectivity is a random variable with a connectivity distribution ranging from 3 to 11. Payatakes and Dias (1984) state that the connectivity value ranges from 4 to 7, acknowledging that it can be as small as 2 and as large as 15. Jerauld *et al.* (1984) showed that as long as the average connectivity of a random connectivity network model is close to the

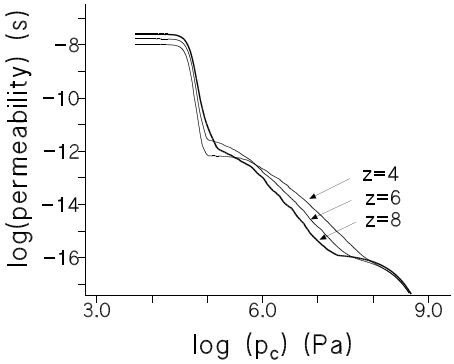

Figure 10. Influence of the connectivity z on the wetting moisture permeability for ceramic brick.

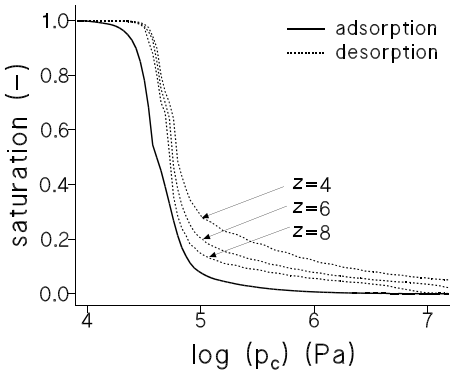

Figure 11. Influence of the connectivity z on the boundary wetting and drying water retention curves. The width of the boundary hysteresis loop increases for pore systems with low connectivity.

constant connectivity of a regular network model, the mass transfer coefficients of both networks are essentially identical. Figure 10 shows the effect of the connectivity on the predicted wetting moisture permeability. Calculations of the permeability function $K(p_c)$ using a 2D square lattice with connectivity $z = 4$, a 2D triangular lattice with a connectivity $z = 6$ and crossed square lattice with a connectivity $z = 8$ are compared. The wetting moisture permeability shows to be less sensitive to value of the connectivity.

The network model can also be used to simulate hysteresis for the boundary drying and wetting water retention curves. However, the hysteresis phenomenon in this model is limited to ink-bottle effects. Contact angle hysteresis is not considered. Hysteresis is found to be present in the entire capillary pressure range (Figure 11). The width of the boundary hysteresis loop increases for pore systems with low connectivity. In Figure 12, the liquid water filling distributions for wetting and drying at a capillary pressure $p_c = 4.9 \times 10^4$ Pa are compared. The distribution for the drying regime clearly shows a fingering effect of dry pores, while the distribution during

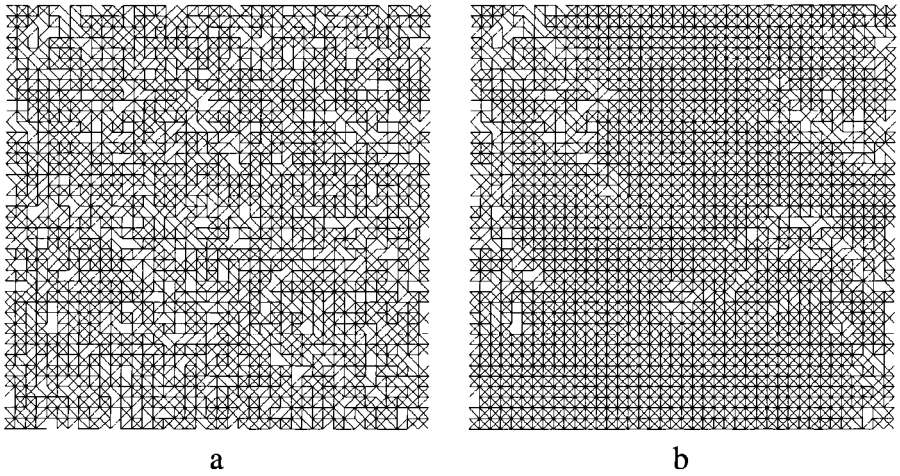

Figure 12. Comparison of the liquid water filling distributions for wetting (a) and drying (b) at a capillary pressure $p_c = 4.9 \times 10^4$ Pa. In drying a fingering effect of the dry pores is observed.

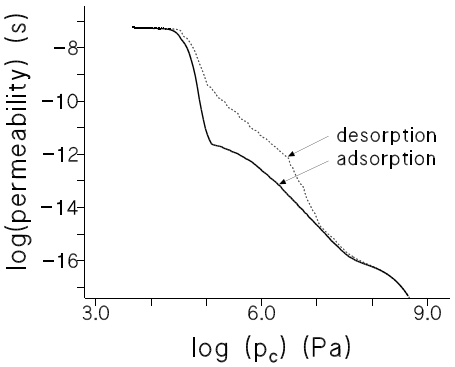

Figure 13. Influence of hysteresis on the moisture permeability versus capillary pressure relation.

wetting is more homogeneous. Figure 13 illustrates the significance of the hysteresis phenomenon on the moisture permeability. The drying moisture permeability is significantly larger due to an increasing availability of continuous flow paths in the drying porous material.

4. Experimental Validation

To test the ability of the multiscale network model to predict the moisture permeability $K(p_c)$, the model results are compared to experimental data. The measurement data include the water retention curve, the moisture permeability and the air permeability of two porous materials: ceramic clay brick and calcium silicate brick.

4.1. PORE VOLUME DISTRIBUTION

Applying Equation (1), the pore volume distribution $f_V(r)$ can be derived from the water retention curve $S(p_c)$. The experimental water retention curve $S(p_c)$ is based on the measured sorption isotherm, pressure plate and mercury intrusion experimental data. In the isothermal sorption experiment an initially dry specimen is conditioned at different relative humidities h and constant temperature until sorption equilibrium is attained between the relative humidity h and the saturation degree S of the specimen. Using Kelvin's equation the sorption isotherm $S(h)$ can be converted into the water retention relationship $S(p_c)$. In a pressure plate experiment a constant air pressure p_a is applied at one side of a water-saturated air-impermeable ceramic plate and a constant water pressure p_l at the other side. A dry specimen is saturated with liquid water under vacuum conditions and brought in contact with this plate. The specimen will desaturate until equilibrium is attained between the applied capillary pressure $p_c = p_a - p_l$ and the saturation S of the specimen. The mercury intrusion test consists of applying a set of increasing pressures to a dry specimen and measuring the corresponding mercury intrusion volume. Knowing the contact angle solid–liquid–gas and surface tension liquid–gas for mercury and liquid water, the mercury intrusion curve can be recalculated into a water retention curve. The water retention curve can be approximated in an analytical form by a sum of power functions (Durner, 1994):

$$S(p_c) = \frac{w(p_c)}{w_{\text{sat}}} = \sum_{i=1}^{k} l_i [1 + (c_i p_c)^{n_i}]^{(1-\frac{1}{n_i})}, \tag{15}$$

where k is the number of power functions and l_i are the weighting factors ($0 < l_i \leqslant 1, \Sigma l_i = 1$). The experimental water retention data are used to determine the distribution parameters by using a Levenberg–Marquadt parameter optimisation algorithm with a least square cost function. Figures 14(a, b) give the water retention curves for calcium silicate and ceramic brick. The estimated parameters are given

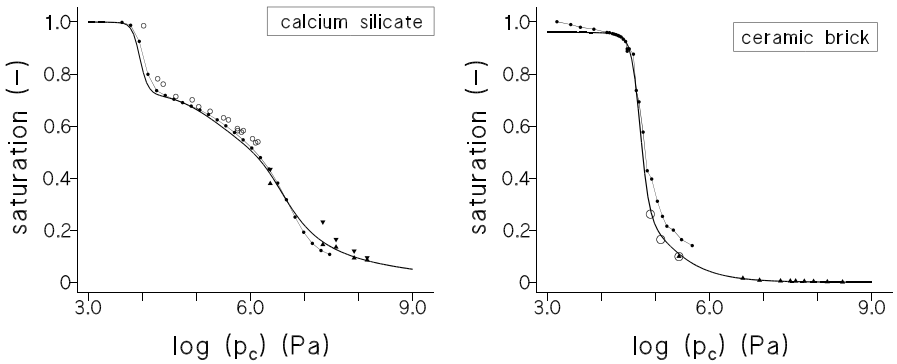

Figure 14. Water retention curve $S(p_c)$: ○, pressure plate; ▲, adsorption isotherm; ▼, desorption isotherm; •—•, mercury intrusion; —, approximated curve for calcium silicate (a) and ceramic brick (b).

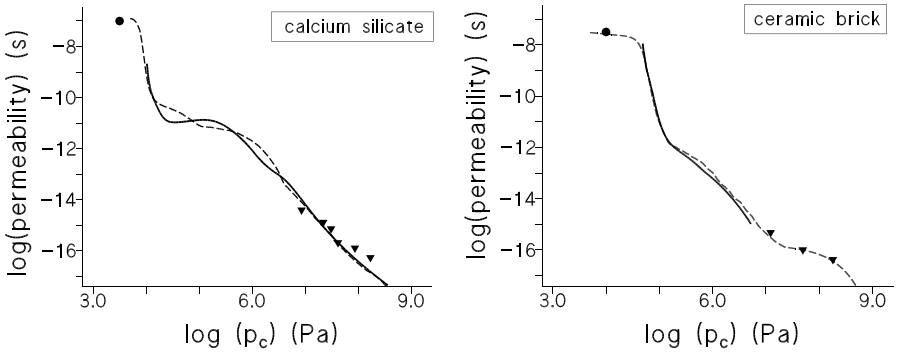

Figure 15. Experimental and simulated moisture permeability versus capillary pressure relationships $K(p_c)$: •, saturated moisture permeability calculated from the measured dry air permeability; —, γ-ray for calcium silicate (a); –, NMR for ceramic brick (b); ▼, wet cup/dry cup vapour permeability; – – –, network simulation.

in Table I. Figure 1 shows the pore volume distributions $f_V(r)$ obtained from the estimated retention curves using Equation (1). The ceramic brick shows a primary coarse pore system and a less important secondary fine-texture pore system in the hygroscopic range. The pore volume distribution of the calcium silicate is characterised by a broad pore system including fine and mid-size pores in the hygroscopic and the capillary range and an important coarse pore system in the capillary range.

4.2. TRANSFER PROPERTIES

The water vapour permeability is determined in an isothermal steady state moisture diffusion experiment. A one-dimensional water vapour flow through the material is created by exposing two opposite surfaces of the specimen to different relative humidity conditions (0.97–0.86, 0.86–0.52 and 0.52–0.11 R.H.). The stationary water vapour flow rate is measured using the cup test method and corrected for the influence of the boundary conditions. From the vapour flow rate the water vapour permeability δ_v (Equation (21)) can be determined. The water vapour permeability $K_v(p_c)$ with respect to p_c can be determined from the measured relation $\delta_v(\phi)$ using Equation (24) (see Appendix). The experimental data are plotted in Figures 15(a, b).

The water diffusivity D_w is determined from the measured transient moisture content profiles in a one-dimensional free imbibition experiment. An initially dry specimen is allowed to adsorb liquid water from a free water surface at one side of the specimen. The moisture profiles are measured using gamma-ray-attenuation (Crausse *et al.*, 1981; Descamps, 1997) or nuclear magnetic resonance (NMR) techniques (Gummerson *et al.*, 1979). The gamma-ray attenuation technique is based on the interaction of gamma-rays with the solid material and water, which results in an attenuation of the incident gamma-ray beam proportional to the moisture content. The NMR technique is based on the manipulation of the magnetic dipole moments of

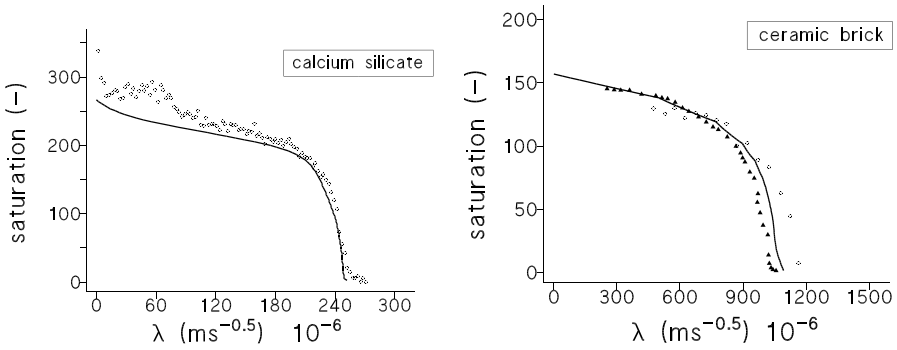

Figure 16. Experimental and calculated Boltzmann $\lambda(w)$ profiles for calcium silicate (a) and ceramic brick (b): ○, γ-ray; ▲, NMR; —, numerical.

the hydrogen nuclei by alternating radio frequency fields, which results in a spin-echo signal with an amplitude proportional to the amount of hydrogen nuclei.

Since the one-dimensional free imbibition experiment approximately fulfils the Boltzmann conditions (semi-infinite homogeneous medium, constant moisture content w_{BC} at the boundary, uniform initial moisture content w_0), the transient moisture content profiles $w(x,t)$ can be transformed into a single $\lambda(w)$-profile, with $\lambda = xt^{-1/2}$ (Boltzmann, 1894 cited in Cranck, 1989). From the transformed moisture profiles, $\lambda(w)$, the water diffusivity D_{w} can be determined by

$$D_{\mathrm{w}}(w) = -\frac{1}{2}\left(\frac{\partial\lambda}{\partial w}\right)_{\mathrm{w}} \int_{w_0}^{w} \lambda(w)\,\mathrm{d}w. \tag{16}$$

Figures 16(a, b) show the measured λ-profiles for calcium silicate and ceramic brick. To determine $(\partial w/\partial\lambda)$ at the moisture content of interest, a spline approximation of the measurement data $\lambda(w)$ is performed (Descamps, 1997). If hysteresis effects in the water retention curve $w(p_c)$ are neglected, the moisture permeability K can be obtained using

$$K = -D_{\mathrm{w}}\frac{\partial w}{\partial p_c}. \tag{17}$$

The air permeability of dry material $K_{\mathrm{a},S=0}$ is experimentally determined in a steady state unidirectional airflow experiment. A dry specimen is exposed to a set of air overpressures $p - p_{\mathrm{atm}}$ and the corresponding airflow is measured (Descamps, 1997). The air permeability $K_{\mathrm{a},S=0}$ is obtained assuming a linear relationship between pressure difference and air flow rate. The saturated water permeability $K_{s=1}$ can be obtained using Equation (13).

4.3. MODEL VALIDATION

Figures 15(a, b) compare the experimental and simulated moisture permeability as a function of the capillary pressure for ceramic brick and calcium silicate. The input

data for the network model are given in Table I. We conclude that the multiscale network with a pore shape ratio $\alpha = -1$ and a connectivity $z = 8$ reasonably identifies the characteristics of the pore space of ceramic brick and calcium silicate brick. The enhancement of the water vapour transfer due to capillary condensation as well as the steep increase of the moisture permeability at a certain capillary pressure are well reproduced.

Finally, the Boltzmann profiles $\lambda(w)$ for a horizontal imbibition problem were calculated using the simulated diffusivity function $D_{\mathrm{w}}(w)$. A fast and accurate semi-analytic algorithm (Philip, 1955) was used to solve the imbibition problem. Due to air entrapment the moisture content will not raise above the so called capillary moisture content w_{cap} (Descamps, 1997). Therefore, the measured capillary moisture content w_{cap} (Table I) is imposed as the boundary moisture content w_{BC} at the imbibition surface. The calculated λ-profiles are compared with the measured λ-profiles using γ-ray and NMR techniques. A good agreement between experiment and simulations is obtained (Figure 16).

5. Conclusions

A multiscale network model has been presented to study the combined water vapour and liquid water transfer in hygroscopic capillary-porous materials with a broad pore-size distribution. Such materials show an important enhancement of the water vapour permeability due to capillary condensation in the porous space, a steep increase of the moisture permeability at a critical moisture saturation and an important hysteresis behaviour.

The multiscale approach is based on the concept of examining the porous space at different levels of magnification. A methodology was developed to estimate the pore radius distributions at each level of magnification introducing a cut-off radius. An isotropic 2D nonplanar cross-squared network model is used to determine the permeability at each level of magnification. Both capillary effects and sorption phenomena, water vapour and liquid water transfer are considered. The conservation of the water vapour permeability of dry material is used as scaling criterion to link the different pore scales. A macroscopic permeability is deduced from the permeabilities predicted at the optimal levels of magnification. An additional measurement of the air permeability of the dry material is necessary to scale the simulated relative moisture permeability to the absolute moisture permeability. A pore shape ratio α is introduced to derive a pore radius distribution from the water retention curve. The value of the pore shape ratio $\alpha = -1$ most closely resembles the behaviour of the considered porous materials. A value of the connectivity $z = 8$ was assumed. It was found that the connectivity z has a minor influence on the wetting behaviour of the material, while in desorption an important influence on the water retention and moisture permeability versus capillary pressure relation was observed. Comparison of the simulated and experimental data demonstrates that the proposed multiscale approach model is able to properly model the highly nonlinear moisture permeability

versus capillary pressure relationship. The network simulates the enhancement of water vapour permeability due to capillary condensation and the steep increase of the moisture permeability at the critical moisture saturation.

In this paper, some assumptions have been introduced. However, these assumptions do not reduce the generality of the present multiscale concept and alternative assumptions can be incorporated. A basic conceptual assumption is that the pore structure does not significantly differ at different levels of magnification. We also assumed that the pore radius distribution at each level of magnification is isotropic without any correlative structure, which is generally not valid. However, when more detailed information on the pore structure is available, a network model using the same multiscale concept can be formulated by using correlated networks at each level of magnification. We are also aware that differences exist between 2D and 3D networks, between networks composed of tubes with volumeless interconnections and sites and bonds networks, mainly because of the trapping phenomenon. These aspects can be accounted for by appropriate modifications in the multiscale model. Also, only isothermal and isobaric conditions were considered. In the nonisothermal case, water vapour diffusion transfer strongly depends on thermal gradients. Consequently, a coupled modelling of heat transfer and moisture transfer is needed. In nonisobaric conditions, the air pressure build-up due to the immiscible displacement of air by water, pressure infiltration processes, air bubbling phenomena and the dissolution of entrapped air may have an important influence on the moisture transfer process.

6. Appendix: Continuum Approach

The pore space is assumed to be partially filled by liquid water (l), which may transform into water vapour (v) forming an ideal mixture with the dry air (a). We limit to moisture transfer under isothermal and isobaric conditions. No bulk air transfer nor advective water vapour transfer takes place. Furthermore, we assume that the porous medium is isotropic, homogeneous and nondeformable. The capillary pressure p_c is defined as the difference of the pressure in the mixture and liquid phase

$$p_c = p_{\text{mix}} - p_{\text{l}}. \tag{18}$$

We assume that Kelvin's law is valid, i.e.,

$$\ln\left(\frac{p_{\text{v}}}{p_{\text{vs}}}\right) = \ln(h) = -\frac{p_c}{\rho_{\text{l}} R_{\text{v}} T}, \tag{19}$$

where h is the relative humidity, p_{v} the water vapour pressure, p_{vs} the temperature dependent saturation vapour pressure, ρ_{l} the density of liquid water, R_{v} the universal gas constant for water vapour and T the absolute temperature. Moisture content is defined as the sum of liquid water and water vapour moisture content $w = w_{\text{l}} + w_{\text{v}}$. The mass conservation principle states

$$\frac{\partial w}{\partial t} = \frac{\partial w_{\text{v}}}{\partial t} + \frac{\partial w_{\text{l}}}{\partial t} = -\text{div}\, \dot{m}_{\text{v}} - \text{div}\, \dot{m}_{\text{l}}, \tag{20}$$

where $\dot{m}_{\text{v}}$ and $\dot{m}_{\text{l}}$ are the density of water vapour and liquid water flow rate.

We assume that the water vapour transfer corresponds to a diffusive water vapour flow trough a nonmoving air phase, which can be described by a Fickian diffusion law

$$\dot{m}_{\mathrm{v}} = -\delta_{\mathrm{v}} \nabla p_{\mathrm{v}}, \tag{21}$$

where δ_{v} is the macroscopic water vapour permeability and $\dot{m}_{\mathrm{v}}$ the density of water vapour flow rate under a partial water vapour pressure gradient ∇p_{v}. The capillary water transfer can be described by Darcy's mass transfer equation

$$\dot{m}_{\mathrm{l}} = -\frac{\rho_{\mathrm{l}}}{\eta_{\mathrm{l}}} B \nabla p_{\mathrm{l}} = K_{\mathrm{l}} \nabla p_{\mathrm{c}}, \tag{22}$$

where $\dot{m}_{\mathrm{l}}$ is the density of the capillary liquid flow rate under a fluid pressure gradient ∇p_{l} or a capillary pressure gradient ∇p_c. K_{l} is the liquid water permeability, η_{l} the dynamic viscosity and B the intrinsic permeability of the porous medium. In Equation (22) gravitational effects are neglected. Using Kelvin's Equation (19), we can rewrite the moisture balance equation in terms of the capillary pressure

$$\frac{\partial w}{\partial t} = \nabla(-K \nabla p_c), \tag{23}$$

where $K = K_{\mathrm{v}} + K_{\mathrm{l}}$ is defined as the moisture permeability and K_{v} is given by

$$K_{\mathrm{v}} = -\delta_{\mathrm{v}} p_{\mathrm{vs}} \frac{\partial h}{\partial p_c}. \tag{24}$$

The relationship between the saturation degree S and the capillary pressure p_c is commonly called the water retention curve $S = S(p_c)$ and is considered a state equation for nondeformable porous media. The moisture saturation is defined as $S = w/w_{\mathrm{sat}}$ where w_{sat} is the saturated moisture content as determined from a vacuum water saturation test.

References

Blunt, M., King, J. M. and Scher, H.: 1992, Simulation and theory of two-phase flow in porous media, *Phys. Rev. A* **46**(12), 7680–7699.

Chandler, R., Koplik, J., Lerman, K. and Willemsen, J. F.: 1982, Capillary displacement and percolation in porous media, *J. Fluid Mech.* **119**, 249–267.

Diaz, C. E., Chatzis, I. and Dullien, F. A. L.: 1987, Simulation of capillary pressure curves using bond correlated site percolation on a simple cubic network, *Transport in Porous Media* **2**(3), 215–240.

Constantinides, G. N. and Payatakes, A. C.: 1989, A three dimensional network model for consolidated porous media: basic studies, *Chem. Engng. Comm.* **81**, 55–81.

Crank, J.: 1989, *The Mathematics of Diffusion*, Oxford University Press, Oxford.

Crausse, P., Bacon, G. and Bories, S.: 1981, Etude fondamentale des transfers couplés chaleur-masse en milieu poreux, *Int. J. Heat Mass Transfer* **24**(6), 991–1004.

Descamps, F.: 1997, Continuum and discrete modelling of isothermal water and air transfer in porous media, PhD Thesis, Catholic University of Leuven, Leuven, Belgium.

Dullien, F. A. L.: 1979, *Porous Media: Fluid Transport and Pore Structure*, Academic Press, New York.

Durner, W.: 1994, Hydraulic conductivity estimations for soils with heterogeneous pore structure, *Water Resour. Res.* **30**, 211–223.

Fatt, I.: 1956, The network model of porous media: III. The dynamic properties of networks with tube radius distribution, *Trans. AIME Petrol. Div.* **207**, 164–177.

Gummerson, R. J., Hall, C., Hoff, W. D., Hawkes, R., Holland, G. N. and Moore, W. S.: 1979, Unsaturated water flow within porous materials observed by NMR imaging, *Nature* **281**, 56–57.

Ioannidis, M. A. and Chatzis, I.: 1993, Network modelling of pore structure and transport properties of porous media, *Chem. Engng. Sci.* **48**(5), 951–972.

Jerauld, G. R., Hatfield, J. C., Scriven, L. E. and Davis, H. T.: 1984, Percolation and conduction on Voronoi and triangular networks: a case study in topological disorder, *J. Phys. C* **17**, 1519–1529.

Kamp, C. L.: 1988, Le transfert d´humidité dans la pâte de ciment durcie, *Chantier Suisse* **19**(5), 419–424.

Koplik, J.: 1982, Creeping flow in two-dimensional networks, *J. Fluid Mech.* **119**, 219–247.

Koplik, J. and Lasseter, T. J.: 1985, Two-phase flow in random network models of porous media, *Soc. Petrol. Engng. J.* **25**, 89–100.

Lenormand, R., Toboul, E. and Zarcone, C.: 1988, Numerical models and experiments on immiscible displacements in porous media, *J. Fluid Mech.* **189**, 165–187.

Lin, C. and Cohen, M. H.: 1982, Quantitative methods for microgeometric modelling, *J. Appl. Phys.* **53**, 4152–4165.

Neimark, A. V.: 1989, Multiscale percolation systems, *Sov. Phys. JETP* **69**(4), 786–791.

Payatakes, A. C. and Dias, M. M.: 1984, Immiscible microdisplacement and ganglin dynamics in porous media, *Rev. Chem. Engng.* 85–174.

Philip, J. R.: 1955, Numerical solution of equations of the diffusion type with diffusivity concentration-dependent, *Trans. Faraday Soc.* **51**, 885–892.

Philip, J. R. and de Vries, D. A.: 1957, Moisture movement in porous materials under temperature gradients, *Trans. Am. Geophys. Un.* **38**, 222–232.

Prat, M.: 1995, Isothermal drying of non-hygroscopic capillary-porous materials as an invasion percolation process, *Int. J. Multiphase Flow* **21**(5), 875–892.

Quenard, D.: 1989, Adsorption et transfer d´humidité dans les matériaux hygroscopiques. Approche du type percolation et expérimentations, PhD Thesis, Institut National Polytechnique de Toulouse, Toulouse, France.

Sahimi, M.: 1993, Flow phenomena in rocks: from continuum models to fractals, percolation, cellular automata, and simulated annealing, *Rev. Modern Phys.* **65**, 1393–1534.

Schirmer, R.: 1938, Die Diffusionszahl von Wasserdampf-Luftgemischen und die Verdampfungsgeschwindigkeit, *VDI Beiheft Verfahrestechnik* **6**, 170.

Soll, W. E. and Celia, M. A.: 1993, A modified percolation approach to simulating three-fluid capillary pressure-saturation relationships, *Adv. Water Res.* **16**, 107–126.

Wilkinson, D. and Willemsen, J. F.: 1983, Invasion percolation: a new form percolation theory, *J. Phys. A* **16**, 3365–3376.

Wilson, K. G.: 1971, Renormalization and critical phenomena, *Phys. Rev. B* **4**(9), 174–184.

Wise, W. R.: 1992, A new insight on pore structure and permeability, *Water Resour. Res.* **28**, 189–198.

Xu, K., Daian, J.-F. and Quenard, D.: 1997, Multiscale structures to describe porous media, Part I: theoretical background and invasion by fluids, *Transport in Porous Media* **26**, 51–73.